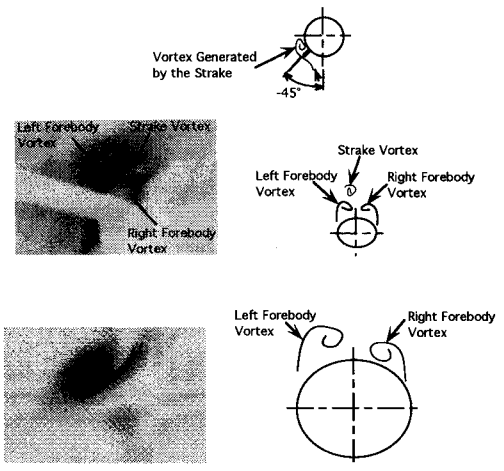

Fig. 4 Off-surface flow visualization for the standard nose with strake A-F at strake angle of −45 deg. Cross section a) 1-1 and b) 3-3.

integration. Results from three different strake roll angles at $\alpha = 50$ deg are shown. The sectional side force coefficients were scaled by their respective total CY (integrated between $\phi = \pm 180$ deg). The results illustrate that approximately 70% of the control power are from the region below the primary flow separation. The control power resulting from the leeward flow is relatively small. The yawing moment is thus generated mainly by asymmetric pressure distribution in the primary flow region. Similar results were obtained for the shark nose.

C. Flow Visualizations

Figure 4 shows the cross-sectional vortex flow patterns of the standard nose with strake A-fwd at a strake angle of −45 deg. At this position, the strake generates a vortex on the right side. At cross section 1-1, three vortices can be observed: one generated by the strake, and the other two are generated at the tip of the forebody. The resultant vortex positions are determined by the relative strengths of the vortices. The vortex from the A-fwd strake is situated farther from the surface than the forebody vortices. The strake vortex is also located closer to the right forebody vortex than the left one, and has the same sense of rotation as the right one. The right vortex is therefore "lifted" from the surface. At cross section 3-3, the asymmetry is amplified. The asymmetry in the forebody vortices is thus reversed from the baseline asymmetry that features a "high" left vortex.

At the strake angle of +45 deg, the strake generates a vortex on the left side. The effect is the opposite of that at $\phi = 45$ deg. The asymmetry in the forebody vortices is thus increased from the baseline asymmetry.

The surface flow visualizations illustrate that the secondary flow separation near the nose tip can be strongly affected by the strake vortex, and there is a strong correlation between the secondary pattern and the vortex asymmetry. The result also illustrates, however, that the primary flow separation lines change only slightly when the strake rotates to different angular positions.

IV. Conclusions

The method was shown to be effective in producing control yawing moments over a wide range of angles of attack. The strake function by acting as a vortex generator, and a vortex is an effective means of controlling other vortices. The strake generates vortices with different trajectories and strength as it rotates to different angular positions on the nose boom. The strake vortex interacts with the forebody vortices near the nosetip. The forebody vortices readjust their orientations due to the interaction. Different velocities and pressures are thereby induced on the two sides of the object by the asymmetric potential vortex flow. Controlled side forces and yawing moments of different magnitudes are therefore generated. The surface pressure integration shows that the side force is generated mostly in the primary flow region.

References

[1]Malcolm, G. N., and Skow, A. M., "Enhanced Controllability Through Vortex Manipulation on Fighter Aircraft at High Angles of Attack," AIAA Paper 86-2277, Aug. 1986.

[2]Malcolm, G. N., Ng, T. T., Lewis, L. C., and Murri, D. G., "Development of Non-Conventional Control Methods for High Angle of Attack Flight Using Vortex Manipulation," AIAA Paper 2192, July 1989.

[3]Malcolm, G. N., and Ng, T. T., "Forebody Vortex Control for Aerodynamic Control of Aircraft at High Angle of Attack," Society of Automotive Engineers Paper 892220, Sept. 1989.

[4]Moskovitz, C., Hall, R., and DeJarnette, F., "Experimental Investigation of a New Device to Control the Asymmetric Flowfield on Forebodies at Large Angles of Attack," AIAA Paper 90-0068, Jan. 1990.

[5]Rosen, B., and Davis, W., "Numerical Study of Asymmetric Air Injection to Control High Angle-of-Attack Forebody Vortices on the X-29 Aircraft," AIAA Paper 90-3004, Jan. 1990.

[6]Tavella, D. A., Schiff, L. B., and Cummings, R. M., "Pneumatic Vortical Flow Control at High Angles of Attack," AIAA Paper 90-0098, Jan. 1990.

[7]Ng, T. T., and Malcolm, G. N., "Aerodynamic Control Using Forebody Blowing and Suction," AIAA Paper 91-0619, Jan. 1991.

[8]Ng, T. T., and Malcolm, G. N., "Aerodynamic Control Using Forebody Strakes," AIAA Paper 91-0618, Jan. 1991.

[9]Ng, T. T., Suarez, C., and Malcolm, G. N., "Forebody Vortex Control with Miniature, Rotatable Nose-Boom Strakes," AIAA Paper 92-0022, Jan. 1992.

[10]Smith, B. C., and Ng, T. T., "Mechanical Control of Vortices on Different F-16 Forebodies Using Miniature Rotatable Strakes," AIAA Paper 94-0048, Jan. 1994.

Shape Sensitivity Analysis of Divergence Dynamic Pressure

Manoj Bhardwaj* and Rakesh K. Kapania†
Virginia Polytechnic Institute and State University, Blacksburg, Virginia 24061

Introduction

In the design of future aircraft, airframe flexibility is a concern from the strength, control, and performance requirements, which need both structural and aerodynamic sensitivity analysis capabilities. Structural sensitivity has been developed over the past two decades for sizing (thickness, cross-section properties) and shape (configuration) variables.[1] Although aerodynamic sensitivity has not existed until recently, a sensitivity does exist for aircraft in subcritical compressible flow,[2] which incorporates disturbances of thickness, camber, or twist distribution. Yates[3] has proposed a new approach that considers general geometry variations including planform for subsonic, sonic, and supersonic unsteady, nonplanar lifting surface theory.

Received May 6, 1993; revision received March 15, 1994; accepted for publication Jan. 15, 1995.

*Graduate Research Assistant, Aerospace and Ocean Engineering. Student Member AIAA.

†Professor, Aerospace and Ocean Engineering. Associate Fellow AIAA.

Aeroelastic sensitivity has existed for two decades with structural sizing variables,[4] which affect the structural stiffness and mass distribution of the airframe, but not its basic geometry. Thus, the sensitivity calculations of the dynamic aeroelastic response have only been available for structural sizing parameters.

In a recent study, Kapania et al.[5] obtained analytically the sensitivity of a wing's flutter response to changes in its geometry. Specifically, the objective was to determine the derivatives of flutter speed and frequency with respect to wing area, aspect ratio, taper ratio, and sweep angle. The study used Giles[6,7] equivalent plate method to represent the wing structure. The aerodynamic loads were obtained using Yates[8] modified strip analysis to analyze flutter characteristics for swept and unswept wings.

In another recent study, Kapania et al.[9] used an analytical approach in determining the sensitivity of the aeroelastic displacements and the trim angle of attack with respect to sweep, wing area, aspect ratio, and taper ratio. An important distinction between the work of Ref. 9 and that of Ref. 5 is that in Ref. 9 a more realistic aerodynamic model, FAST (Ref. 3), was incorporated. FAST incorporates a lifting surface theory rather than a lifting line theory used in Ref. 9.

Barthelemy and Bergen[10] conducted a study and calculated semianalytically the sensitivity derivatives of wing static aeroelastic characteristics with respect to wing-shape parameters. The study provided results showing that semianalytically calculated sensitivities are less expensive than those calculated by the finite difference approach. The study of Ref. 10, however, used Weissinger's L-method for aerodynamic prediction, as opposed to FAST used in the present study.

This Note presents methods for determining the sensitivity of divergence dynamic pressure with respect to 1) sweep, 2) wing area, 3) aspect ratio, and 4) taper ratio. The formulation is quite general so that it may be used in conjunction with any aerodynamic and structural analysis packages.

General Equations

The divergence dynamic pressure is found from the eigensolution of the system of equations

$$[[I]\lambda - [B]]\{X\} = \{0\} \tag{1}$$

and the adjoint problem

$$[[I]\lambda - [B]^T]\{Y\} = \{0\} \tag{2}$$

where X is the right-hand eigenvector, Y is the left-hand eigenvector, λ are the eigenvalues, and

$$[B] = [K]^{-1}[A]\left[\frac{\partial\{a\}}{\partial\{C\}}\right] \tag{3}$$

where $[K]^{-1}$ is the inverse of the stiffness matrix, $[A]$ is the aerodynamic kernel matrix, and $[\partial\{a\}/\partial\{C\}]$ is the derivative of the generalized pressure coefficients wth respect to generalized displacements as developed in Ref. 9. The divergence dynamic pressure q_D was equal to the inverse of the largest positive real eigenvalue

$$q_D = 1/\lambda_i \tag{4}$$

The divergence dynamic pressures were calculated for the various wing parameters. The sensitivities of the eigenvalues were calculated at the base configuration, which is a wing area of 15 m^2, an aspect ratio of 3.75, a taper ratio of 0.5, a quarter-chord sweep of 5 deg, with a root α_0 of 5.769, and no twist.

The sensitivity of the eigenvalue λ as given by Lancaster,[11] is

$$\frac{\partial\lambda}{\partial r} = \frac{\{Y\}^T\left[\frac{\partial[B]}{\partial r}\right]\{X\}}{\{Y\}^T\{X\}} \tag{5}$$

where r is the shape parameter in concern, and

$$\frac{\partial[B]}{\partial r} = \frac{\partial[K]^{-1}}{\partial r}[A]\left[\frac{\partial\{a\}}{\partial\{C\}}\right] + [K]^{-1}\frac{\partial[A]}{\partial r}\left[\frac{\partial\{a\}}{\partial\{C\}}\right] + [K]^{-1}[A]\frac{\partial\left[\frac{\partial\{a\}}{\partial\{C\}}\right]}{\partial r} \tag{6}$$

where $\partial[K]^{-1}/\partial r$ is calculated as follows:

$$[K]^{-1}[K] = [I]$$

and now differentiating gives

$$\frac{\partial[K]^{-1}}{\partial r}[K] + [K]^{-1}\frac{\partial[K]}{\partial r} = [0]$$

which reduces to the following:

$$\frac{\partial[K]^{-1}}{\partial r} = -[K]^{-1}\frac{\partial[K]}{\partial r}[K]^{-1} \tag{7}$$

and since $q_D = 1/\lambda_i$

$$\frac{\partial q_D}{\partial r} = -q_D^2\frac{\partial\lambda}{\partial r} \tag{8}$$

where $\partial[K]/\partial r$ and $\partial[\partial\{a\}/\partial\{C\}]/\partial r$ are calculated using finite difference methods while $\partial[A]/\partial r$ is calculated analytically.

Results

Figures 1–4 show the sensitivities of divergence dynamic pressure with respect to wing-shape parameters. The solid lines show q_D vs r, where r is a shape parameter and q_D is divergence dynamic pressure calculated using Eq. (4). The dashed lines are the sensitivities plotted at the baseline configuration. The graphs show that the sensitivities are very close to tangency to the solid curves, which indicate good results, because the exact sensitivities would be tangent to the solid curves. The graphs show the sensitivities calculated are very good, even if the baseline configuration changes by as much as 20% of its initial shape parameters. If a bigger change occurs in the baseline configuration, the sensitivities should be recalculated.

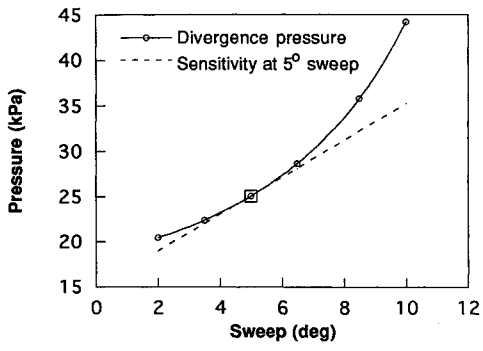

Fig. 1 Sensitivity of divergence dynamic pressure with respect to sweep at baseline configuration.

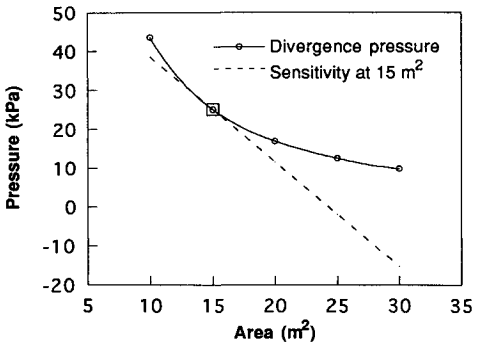

Fig. 2 Sensitivity of divergence dynamic pressure with respect to area at baseline configuration.

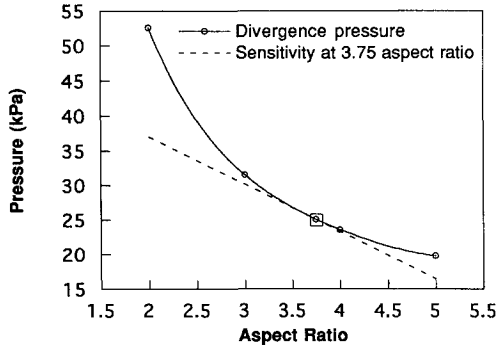

Fig. 3 Sensitivity of divergence dynamic pressure with respect to aspect ratio at baseline configuration.

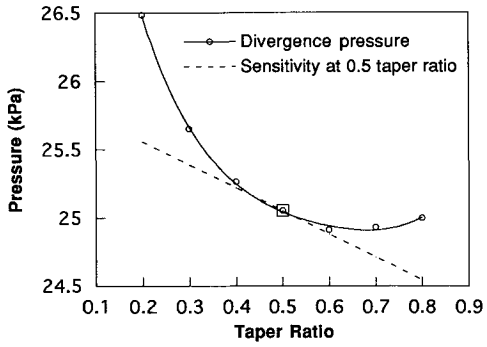

Fig. 4 Sensitivity of divergence dynamic pressure with respect to taper ratio at baseline configuration.

The calculation of $\partial[\partial\{a\}/\partial\{C\}]/\partial r$ took the majority of time in this study. This was due to the fact that $\partial[\partial\{a\}/\partial\{C\}]/\partial r$ was calculated by a central finite difference method. This required many calculations of $[\partial\{a\}/\partial\{C\}]$ in determining the optimal step size. The evaluation of $[\partial\{a\}/\partial\{C\}]$ at each configuration took approximately 35 min, and for every step size two new calculations were needed, thus consuming the majority of the time in sensitivity calculations.

It should be noted that the partial differentiation of the stiffness matrix $[K]$ was obtained using a finite difference method. Due to the simplicity of coding, $\partial[K]/\partial r$ was calculated using a finite difference method as opposed to analytic calculation. However, this does not have a major affect on the study because the main problem is the time consumption in the calculation of $\partial[\partial\{a\}/\partial\{C\}]/\partial r$, and not $\partial[K]/\partial r$.

In this study the sensitivities are calculated semianalytically. However, there has been an ongoing effort at NASA Lewis Research Center (LRC) to calculate the $\partial[\partial\{a\}/\partial\{C\}]/\partial r$ analytically. Once this has been done, this study could be used to validate those results obtained from a completely analytical study.

Conclusions

In the design phase of an engineering system, it is very important to know how perturbing a certain input parameter will affect an output variable of concern. These sensitivities can help the designer optimize a configuration with respect to certain parameters. If the configuration has changed by a certain amount, the sensitivities are recalculated and may need to be recalculated numerous times. Currently, to obtain these sensitivities, a finite difference method is used, but finite difference methods can incur truncation and round-off errors, not to mention the time consumed in finding an optimal step size. Especially if the function evaluation is expensive or time-consuming, as was the case in this study.

Due to the time consumption of a finite difference method, this study questions if an analytical approach can be implemented to calculate sensitivities, specifically the sensitivities of divergence dynamic pressure with respect to sweep, area, taper ratio, and aspect ratio. At the time of the study, it was believed that all the tools necessary to do this were available. It was found later that the analytical calculation of $\partial[\partial\{a\}/\partial\{C\}]/\partial r$ is still being developed at NASA LRC. Therefore, this study falls short of its objective, and the sensitivities are calculated semianalytically, but this study still proves to be a valuable tool.

This study takes a step in the right direction in showing that there is potential of calculating sensitivities analytically. The time consumed to calculate sensitivities by a finite difference method can be reduced significantly using an analytical approach. Also, one avoids truncation and round-off errors that occur when using a finite difference approach. Therefore, the analytical calculation of sensitivities provides more accurate results in less time. In addition, if and when the analytical calculation of $\partial[\partial\{a\}/\partial\{C\}]/\partial r$ is developed, this study could be used for validation purposes.

Acknowledgments

Portions of this work were performed under Grant NAG-1-1411 from NASA Langley Research Center, with J.-F. Barthelemy as the Grant Monitor. Also, the authors would like to thank Lloyd Eldred, from Wright–Patterson Air Force Base, for his continuous help during this study.

References

[1]Adelman, H. M., and Haftka, R. T., "Sensitivity Analysis of Discrete Structural Systems," *AIAA Journal*, Vol. 24, No. 5, 1986, pp. 823–832.

[2]Hawk, J. D., and Bristow, D. R., "Development of MCAERO Wing Design Panel Method with Interactive Graphics Module," NASA CR-3775, April 1984.

[3]Yates, E. C., Jr., "Aerodynamic Sensitivities from Subsonic, Sonic, and Supersonic Unsteady, Nonplanar Lifting Surface Theory," NASA TM-100502, Sept. 1987.

[4]Haftka, R. T., and Yates, E. C., "Repetitive Flutter Calculations in Structural Design," *Journal of Aircraft*, Vol. 13, No. 7, 1976, pp. 456–461.

[5]Kapania, R. K., Bergen, F. D., and Barthelemy, J.-F. M., "Shape Sensitivity Analysis of Flutter Response of a Laminated Wing," *Proceedings of the AIAA/ASME/ASCE/AHS/ASC 30th Structures, Structural Dynamics, and Materials Conference*, 1989, pp. 920–932.

[6]Giles, G. L., "Equivalent Plate Analysis of Aircraft Wing Box Structures with General Planform Geometry," *Journal of Aircraft*, Vol. 23, No. 11, 1986, pp. 859–864.

[7]Giles, G. L., "Further Generalization of an Equivalent Plate Representation for Aircraft Structural Analysis," *Journal of Aircraft*, Vol. 26, No. 1, 1989, pp. 67–74.

[8]Yates, E. C., "Calculation of Flutter Characteristics for Finite-Span Swept or Unswept Wings at Subsonic and Supersonic Speeds by A Modified Strip Analysis," NASA RM L57110, March 1958 (Declassified Feb. 6, 1962).

[9]Kapania, R. K., Eldred, L. B., and Barthelemy, J.-F. M., "Sensitivity Analysis of a Wing Aeroelastic Response," *Proceedings of the AIAA/ASCE/ASME/AMS/ASC 32nd Conference on Structures, Structural Dynamics, and Materials Conference* (Baltimore, MD),

1991; also *Journal of Aircraft*, Vol. 30, No. 4, 1993, pp. 496–504.

[10]Barthelemy, J.-F. M., and Bergen, F. D., "Shape Sensitivity Analysis of Wing Static Aeroelastic Characteristics," NASA TP 2808, May 1988; see also *Journal of Aircraft*, Vol. 26, No. 8, 1989, pp. 712–717.

[11]Lancaster, P., "On Eigenvalues of Matrices Dependent on a Parameter," *Numerische Mathematik*, Vol. 6, No. 5, 1964, pp. 377–387.

Improvement of Transonic Wing Buffet by Geometric Modifications

Shen-Jwu Su*
Aero Industry Development Center, Taichung, Taiwan, Republic of China
and
Chuen-Yen Chow†
University of Colorado, Boulder, Colorado 80309-0429

Introduction

WING buffet is a result of boundary-layer separation on the wing. Buffeting in transonic flow regime is closely connected with the shock-induced boundary-layer interaction, which can either cause boundary-layer separation beneath the shock leading to a separation bubble, or result in an early rear separation due to the increased susceptibility of the post-shock boundary layer in an adverse pressure gradient.[1] Both types of flow separation cause fluctuations in aerodynamic forces to stimulate the aircraft structure, and thus lead to limitations in the flight envelope of the aircraft.

The buffet boundary is the boundary in the lift (or angle of attack) and freestream Mach number plane separating conditions where the flow is essentially attached and where the flow is totally separated and dominated by shock oscillations and large pressure fluctuations. Most of the earlier studies of buffet were relied on wind-tunnel tests, and the method to determine buffet for airfoil or wing was approached by looking for the first slope decreasing in the C_l-α plot. However, many difficulties to accurately simulate buffeting arise from the experimental side, which include the rigidity of test models, the number of influential parameters being too large, lengthy time, and expensive cost of experiments, etc. A more economical and less time-consuming alternative to the determination of buffet boundaries would be the computational method, which is adopted for the present study.

Theoretically, the buffet onset of a transonic wing can be raised if boundary-layer separation and shock-wave strength are favorably controlled by making appropriate modifications to the wing geometry. Studies of conventional airfoils[2,3] and supercritical airfoils[4] with flaps show that the buffet boundaries can be raised appreciably by applying proper flap settings. More recently, Henne and Gregg[5] examined the geometric properties of a supercitical airfoil and found that a finite trailing-edge thickness can provide increased lift and also improvement in the wing buffet onset characteristics. To gain more insight into the possibilities of using geometric variation as a means for improving transonic buffeting, numerical investigations are carried out to study the performance of a twisted wing and that of a step wing with conventional symmetric airfoil sections.

A numerical tool has been assembled particularly for analyzing the wing buffet phenomenon, which consists of a three-dimensional grid-generation package and an efficient flow solver. The latter is based on an implicit finite difference code for solving the thin-layer compressible Navier–Stokes equations, using the Baldwin–Lomax turbulence model for boundary-layer calculations. A two-factored flux-split scheme is employed, which has the ability to compute subsonic, transonic, and supersonic flows about wings of arbitrary shape with possible weak boundary-layer separation. A detailed description of this numerical scheme is referred to in Pulliam and Steger.[6]

The wing model used for the analysis here is based on the ONERA M6 wing[7] configuration shown in Fig. 1. This untwisted wing of symmetric airfoil sections was developed especially for the experimental support of three-dimensional transonic and subsonic flowfield studies, whose extensive database of surface pressure distribution is available over a range of transonic Mach numbers at angles of attack up to 6 deg.

The computational grids are generated in the C-O topology (C in the streamwise direction and O in the spanwise direction). The total number of grids is 195 × 30 × 49. Either the algebraic or elliptic grid solver may be employed for surface and volume grid generation. Boundary-fitted meshes are generated with adequate spacing in the viscous sublayer to accurately resolve the high Reynolds number turbulent flow. In addition, grid refinements in the shock and wingtip regions are implemented for solving the transonic buffet problem.

Prediction of Light Buffeting

The light buffeting calculation for finite wings (reference to Thomas' idea concluded from the behavior of boundary-layer separation during buffeting) was made by Proksch.[8] The buffeting boundary is determined by taking into account the differential spanwise loading of the wing. For this purpose, a buffeting coefficient C_{bi} is introduced, which is directly related to the rms value of the wing root bending moment

$$C_{bi} = \int_{\eta_R}^{1} \frac{C_s(\eta)}{\bar{C}} (\eta - \eta_R)\, d\eta \tag{1}$$

in which $\bar{C}$ is a reference chord of the wing given by

$$\bar{C} = \frac{2}{3} C_r \left(\frac{1 + \lambda + \lambda^2}{1 + \lambda} \right) \tag{2}$$

where λ is the taper ratio of C_t/C_r, and C_t, C_r are the chords at the tip and root of the wing.

Equation (1) is established by assuming that the fluctuations of the wing root bending moment are proportional to the integral, evaluated along the wingspan, of the product of local lift fluctuations and the distance $(\eta - \eta_R)$ from the wing root. A further assumption is that the local lift oscillations caused by flow separation are proportional to the chord length $C_s(\eta)$ of the separated flow at a station of the wing. It has been shown[9] that a value of C_{bi} from 0.08 to 0.1 will coincide with the measured buffeting boundary. The value $C_{bi} = 0.09$ is used here as the criterion for buffet onset based on the slope method described earlier. In the neighborhood of this value the slope $dC_l/d\alpha$ consistently starts to decrease as shown in our computed results for various wing configurations.

Buffet Improvement

Transonic computations for the baseline M6 wing show that, at buffet onset, some shock-induced separation bubbles

Received June 6, 1993; presented as Paper 93-3024 at the AIAA 23rd Fluid Dynamics Conference, Orlando, FL, July 6–9, 1993; revision received Oct. 12, 1994; accepted for publication Jan. 30, 1995.

*Computational Fluid Dynamics Group Leader, Aeronautical Research Laboratory, Aerodynamics Department.

†Professor, Department of Aerospace Engineering Sciences. Associate Fellow AIAA.